J Appl Electrochem (2013) 43:279–287
DOI 10.1007/s10800-012-0509-y

ORIGINAL PAPER

Ni-doped TiO_2 hollow spheres as electrocatalysts in water electrolysis for hydrogen and oxygen production

Jayeeta Chattopadhyay · Rohit Srivastava · P. K. Srivastava

Received: 11 August 2012 / Accepted: 12 November 2012 / Published online: 29 November 2012

Abstract This work represented the electrocatalytic properties of Ni-doped titania hollow sphere materials in hydrogen and oxygen evolution during water electrolysis from acidic media. Titania hollow sphere particles were synthesized using poly(styrene-methacrylic acid) latex as template material, and various amount of nickel were doped over the sphere using nickel (II) sulfate as the precursor of nickel. The presence of rutile TiO_2 and NiO phases were revealed during XRD analysis, indicating the critical growth of nickel on the surface of the hollow sphere catalysts. BET surface area results also shown the 166.76 $m^2\ g^{-1}$ value for 30 wt% Ni/TiO_2 hollow sphere sample. The SEM and TEM images were confirmed the hollow sphere structure of the catalysts with diameter of 0.8–0.9 μm. The cyclic voltammetric studies proved the presence of both hydrogen and oxygen evolution peaks for all the hollow sphere samples. The anodic peak current density value, which usually represents the oxygen evolution phenomenon, was revealed as 13 mA cm^{-2} for 25 wt% Ni-loaded sample; whereas, the hydrogen evolution peak was most intense for 30 wt% Ni/TiO_2 material with cathodic peak current density of 32 mA cm^{-2}. The average value of −1.42 were determined as the reaction order of the system irrespective of the nickel loading and heating duration in the synthesis of hollow sphere materials. During photocatalytic water splitting, 30 wt% Ni/TiO_2 hollow sphere sample yielded the highest amount of hydrogen in all irradiation time span.

J. Chattopadhyay (✉) · R. Srivastava · P. K. Srivastava
Department of Applied Chemistry, Birla Institute of Technology, Deoghar Extension Campus, Jasidih 814 142, Jharkhand, India
e-mail: jayeeta08@gmail.com

Keywords Ni-doped titania · Hollow sphere · Electrocatalysts · Water electrolysis

1 Introduction

Today energy consumers on earth are heavily dependent on air polluting fossil fuels, and with the present production rate, out energy reservoirs could be emptied in less than a couple of 100 years [1]. So far, around two billion people in the world do not have access to electricity [2]. Providing such a number of people with electricity will have a major effect on the environment, if fossil fuels are only used. The requirement for new energy carrier is well established, and the world's current use of hydrocarbons as a primary energy source is not sustainable [3]. Hydrogen is considered as a novel fuel for the twenty-first century, mainly due to its environmentally benign character. It is widely acknowledged that hydrogen is an attractive energy source to replace conventional fossil fuels, both from the environmental and economic standpoint. When hydrogen is used as a fuel it generates no pollutants, but produces water which can be recycled. Water electrolysis represents a most important process, which offers the way to convert electrical energy to chemical energy as hydrogen and oxygen production. The key components of all electrochemical cells are electrodes and separators [4]. In almost all the cases where process economics require the optimization of cell performance, electrodes and/or electrocatalysts of noble metals or their oxides are the components of choice in water electrolysis for hydrogen and oxygen production irrespective of their high cost. In the last decade, several scientists have been engaged in the fuel cell research seeking to develop catalysts resistant to CO and acid that could replace platinum as anode catalyst. The high price

and limited supply of Pt also constitute a major barrier to the development of the suitable electrocatalysts in various kinds of electrochemical reactions and fuel cells.

Titania dioxide has been the most widely used pigment powder to achieve whiteness and opacity in products like cosmetics, coatings, or paper. Moreover, great interest is attached to their functional ceramic layers and electrical properties. Its characteristics, like, high dielectric constant, purity and homogeneity made the semiconductor titanium dioxide become increasingly important as electrode material in a variety of applications. Recently, the reduction of molecular oxygen at titanium dioxide electrodes has also been widely studied in connection with titania as cathode material. The reduction of oxygen, whether in a $2e^-$ or $4e^-$ transfer, plays an important role in electrochemical technology and is especially interesting for applications in fuel cells, batteries, or cathodic reactions during electrolysis, and of course for the rudimental understanding of artificial systems, too [5]. Since titanium dioxide is an attractive and low-cost compound in electrocatalysis, i.e., by enhancing the catalytic activity of metallic catalysts by a strong metal support interaction (SMSI effect), or by the development of mixed oxide [6, 7] or defining oxides with metal complex [8–10], new properties can be achieved. TiO_2 offers several attractive features such as a low volume change ($\sim$4 %) during the charge–discharge process, low production cost, low toxicity, and the ability to be prepared as nanotubes, nanowires, nanoparticles, and mesoporous structures.

Now-a-days, nano- and submicron-sized inorganic materials with specific structural features have attracted much attention for their intriguing physical properties due to unusual sizes and shapes [11–13]. Among them, the spherical hollow structures certainly provide advantageous features, e.g., low density, large surface area, and void volume with tunable shell thickness, so that they would provide a wide range of potential applications in catalysis, biomedicine, magnetic recording media, and ferrofluid technology for their unique properties [14, 15]. One of the most useful methods to synthesize hollow spheres with a monodispersed size distribution is soft template synthesis [16–18], in which template core particles, such as polystyrene (PS) beads, are coated with inorganic substances, and then removed by solvent liquation or calcination. Titania hollow spheres and their unique properties have been studied extensively by many researchers with the application in photocatalytic reactions [19]. But very few have applied the hollow spherical form of titania as electrocatalysts. In our previous works, we have synthesized tin [20] and barium [21]-doped titania hollow sphere employing sulfonated poly styrene (PS) latex particles as template material. In the present study, we have prepared nickel-doped titania hollow spheres using the same procedure, and evaluate their electrocatalytic properties in water electrolysis in acidic media. Nickel has been chosen as suitable electrocatalysts by many scientists due to its inexpensive nature [22]. Few works have been mentioned in the literature for nickel hollow spheres as electrocatalysts. Xu et al. [23] had reported about the synthesis of nickel hollow sphere, and they applied them in methanol and ethanol electro-oxidation in alkaline media. Nishida et al. [24] had synthesized nanometer-sized nickel catalysts supported on hollow spherical particles of samaria-doped ceria (Ni/SDC), which was aimed for solid oxide fuel cell (SOFC) anode applications. We present here a facile synthesis of hollow core–shell masoporous titania hollow sphere, with the further doping by nickel. We have examined the applicability of nickel-doped TiO_2 hollow spheres as electrocatalysts in hydrogen and oxygen evolution reaction during water electrolysis.

2 Materials and methods

2.1 Hollow sphere synthesis

Titania hollow spheres were synthesized using poly(styrene-methacrylic acid) latex particles as template material, containing carboxylic groups on its surface. The PSA latex spheres were prepared following the method reported earlier in our previous work [20, 21]. The diameter of the PSA latex sphere particles was 500–560 nm. During the synthesis, pure TiO_2 hollow sphere particles, $Ti(SO_4)_2$ (Sigma-Aldrich, USA) has been used as the precursor material. The synthesis process and the materials used were exactly similar as we had reported earlier [20, 21]. After the preparation of pure titania hollow spheres, 15, 25, and 30 wt% of nickel was loaded over the spheres. During the preparation, requisite amount of TiO_2 was added into 32 ml of distilled water under vigorous stirring followed by the addition of 0.8 ml of HCl (CDH, India), 1.98 ml of CTACl (ACM Chemicals, India), and the appropriate amount of nickel (II) sulfate (Merck, India). The mixture was then aged at 70 °C. After aging of 12 h, it was cooled, centrifuged, and washed with distilled water. The obtained materials were then calcined at 400 °C. The 25 wt% Ni/TiO_2 hollow sphere sample was treated separately with 300, 400, and 500 °C calcinations temperatures.

2.2 Characterizations of hollow spheres

The X-ray diffraction patterns were examined by a D/MAX—3C equipment of Rigaku Denki Co. Ltd. using Cu Kα radiation with fixed powder source (30 kV, 15 mA); the applied scan rate was 2° (2θ)/min. Specific surface areas of the catalysts were measured by Brunauer–Emmett–Teller (BET) surface area analysis with Micromeritics ASAP

equipment, model 2010 using N_2 adsorption–desorption isotherms at 77.35 K. The thermogravimetric analysis (TGA) was studied using Shimadzu TGA-50H apparatus, by heating the samples up to 700 °C with the 10 °C/min heating rate under air atmosphere (25 ml/min). The surface morphologies of the hollow sphere samples were measured using scanning electron microscope (SEM) and transmission electron microscope (TEM) with JSM-6400 and JEM-2010, respectively.

2.3 Electrochemical measurements

The hollow sphere catalyst ink was prepared using Nafion® solution (Aldrich, USA), water and i-propyl alcohol using the same method as mentioned in our earlier works [20, 21]. Approximately 2 mg of catalyst was loaded onto the water-proofed carbon cloth (1 cm × 1 cm). Electrochemical measurements were carried out in a three-electrode cell with Potentiostat/Galvanostat (Princeton Applied Research, Parastat® 4000) using Ag/AgCl in 3 M KCl solution as reference electrode and Pt plate (1 cm × 1 cm) as counter electrode in 0.1 N H_2SO_4 solution. The cyclic voltammetric measurements were performed in the potential range of −1.2 to 2.0 V with a scan rate of 40, 80, and 100 mV s^{-1}. The anodic polarization and Tafel slopes were recorded with a potential scan rate of 0.5 mV s^{-1}.

2.4 Photochemical measurements

The photocatalytic hydrogen evolution reactions were carried out in a 5 ml quartz reactor. 2.1 mg of the hollow sphere catalyst was suspended in a solution of 2 ml of water and 0.5 ml of methanol. A 300 W Xenon lamp attached with an optical transmission filter >280 nm was utilized as the AM 1.5 simulated light source. To eliminate the dissolved oxygen prior to light irradiation, the suspension was degassed with Ar for 20 min. The amount of hydrogen produced was measured by molecular sieve column and a TCD detector.

3 Results and discussions

3.1 Structural and thermal characterizations of hollow spheres

3.1.1 XRD analysis

Figure 1 shows the XRD patterns of Ni-doped TiO_2 hollow sphere electrocatalysts with three various compositions calcined at 400 °C. The results illustrate the presence of NiO and rutile TiO_2 phase on the catalyst surface. Diffraction peaks around 38°, 43°, and 67° were found, which

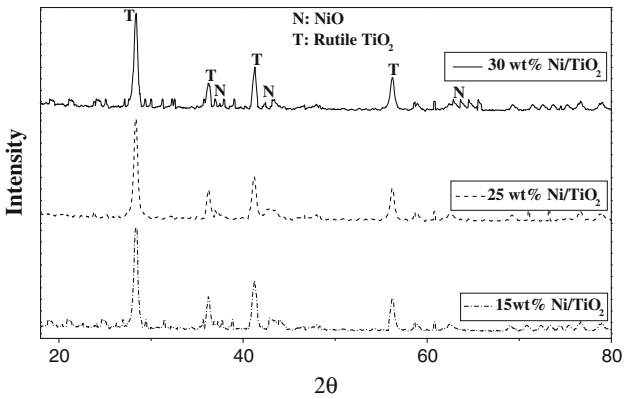

Fig. 1 XRD patterns of 15, 25 and 30 wt% Ni-doped TiO_2 hollow spheres calcined at 400 °C temperature

are ascribed to (111), (200), and (220) planes of NiO phase, respectively [25]. At the same time, the peaks for rutile TiO_2 phase were formed around 28° (110), 36° (101), 41° (111), and 55° (211) [20, 21, 26]. The only presence of rutile TiO_2 phase without showing any crystalline peak for anatase phase in the hollow spheres indicates the stability of the electrocatalysts during water electrolysis, as this phase is known as stable matter in strong acidic or basic solution. Here, we can see that the peak intensity has not changed much for NiO phase with variation in the composition of catalysts, but rutile titania phase is more intense for the hollow spheres with less nickel loading.

3.1.2 TG analysis

Thermogravimetric curve of 25 wt% Ni/TiO_2 hollow sphere sample (without heat treatment) is shown in Fig. 2. The thermal analysis was carried out by heating the sample

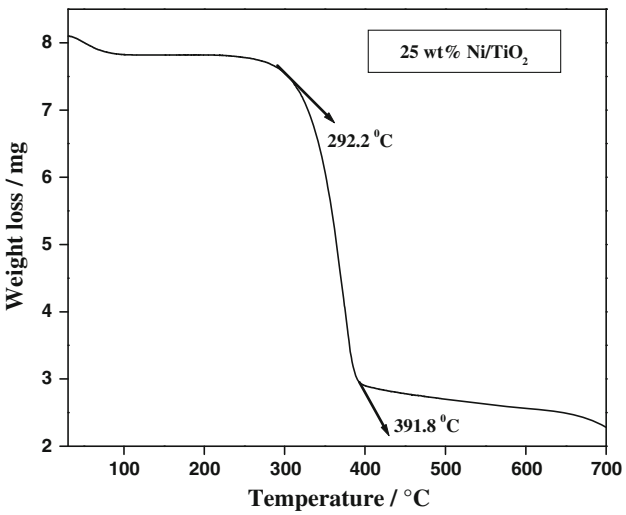

Fig. 2 TGA study of 25 wt% Ni/TiO_2 hollow sphere without heat treatment

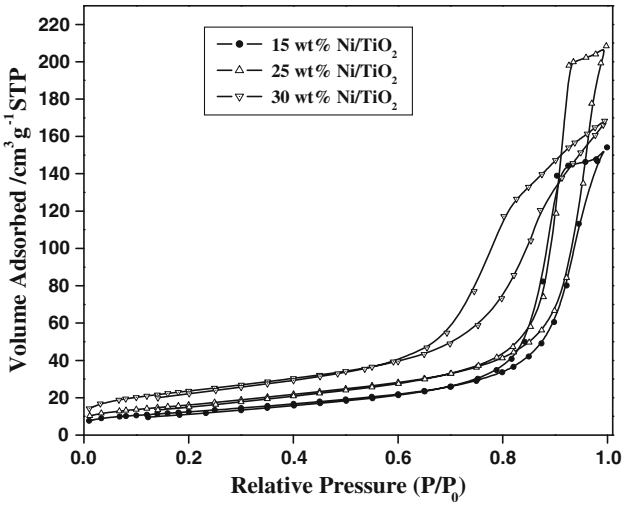

Fig. 3 N_2 adsorption isotherms of 15, 25, and 30 wt% Ni/TiO_2 hollow spheres calcined at 400 °C temperature

up to 700 °C with the heating rate of 10 °C min^{-1}. The curve has shown rapid weight loss between 292 and 392 °C, and further the degradation went on up to 600 °C. The whole weight loss phenomena can be attributed to several mechanisms, which were situated simultaneously during the heat treatment. The initial weight degradation can be assigned for the water evaporation from the catalyst, which was further continued in the burning out of organic residues such as PSA latex and surfactant cetyltrimethylammonium chloride (CTACl).

3.1.3 BET surface area and isotherm

The nitrogen adsorption isotherms of Ni-doped titania hollow sphere catalysts are presented in Fig. 3. All the hollow sphere samples are exhibiting the typical type IV isotherm, which are the characteristics of mesoporous solids [27]. The results of surface area and pore size distribution are summarized in Table 1. The results have shown the BET surface area values of 110.52, 152.31, and 166.76 $m^2\ g^{-1}$ for 15, 25, and 30 wt% Ni-loaded hollow sphere sample (calcined at 400 °C), respectively. Similarly, 25 wt% Ni/TiO_2 hollow sphere samples calcined at 300 and 500 °C have exhibited the BET surface area value of 43.22 and 88.17 $m^2\ g^{-1}$, respectively. The results are indicting the declination of surface area values with raising or lowering of calcinations temperature of hollow sphere samples. Actually, calcinations at 300 °C do not initiate the surface cracking, resulting in the lower surface area result. Similarly, hollow sphere structure did not exist for the sample with 550 °C calcinations temperature. Average pore diameter value is evaluated highest for 30 wt% Ni-doped titania hollow sphere sample.

Table 1 BET surface area and pore size results of Ni/TiO_2 hollow spheres

Sample	BET surface area ($m^2\ g^{-1}$)	Langmuir surface area ($m^2\ g^{-1}$)	Average pore diameter (4 V/A)/ A°	BJH adsorption average pore diameter (4 V/A)/A°
15 wt% Ni/TiO_2 (calcined at 400 °C)	110.52	143.23	117.23	110.25
25 wt% Ni/TiO_2 (calcined at 400 °C)	152.31	201.1	176.25	175.2
30 wt% Ni/TiO_2 (calcined at 400 °C)	166.76	211.52	189.55	181.84
25 wt% Ni/TiO_2 (calcined at 300 °C)	43.22	86.28	156.27	149.85
25 wt% Ni/TiO_2 (calcined at 500 °C)	88.17	108.36	190.41	189.55

3.1.4 TEM and SEM analysis

The SEM image of 30 wt% Ni/TiO_2 hollow sphere calcined at 400 °C is presented in Fig. 4. Similarly, Fig. 5 is the TEM images of 30 wt% Ni-doped titania hollow sphere electrocatalysts calcined at 400 °C. SEM and TEM results are showing a uniform layer of nickel over the spherical structure, with the average sphere diameter of 0.8–0.9 μm of size; although some bare titania surface also exists in the catalysts. The nickel particles size is revealed as 10–65 nm.

3.2 Electrochemical characterizations

3.2.1 Cyclic voltammetric measurements

The electrocatalytic activity of Ni/TiO_2 hollow spheres with various compositions of nickel have been measured using cyclic voltammetric (CV) analysis with the scan rate of 100 mV s^{-1}. Figure 6 is representing the typical voltammograms of hollow sphere electrocatalysts. In the CV curves, two anodic peaks (a_1 and b_1) and only one cathodic peak (a_2) are situated. 25 wt% Ni/TiO_2 sample has produced the highest anodic peak current density value of 13 mA cm^{-2}. It has shown reduced value of 12 mA cm^{-2} for 15 wt% Ni-loaded hollow sphere catalyst, which was further decreased to 10.2 mA cm^{-2} for 30 wt% Ni/TiO_2 sample. The large void space formed inside the hollow sphere structure has enhanced the oxygen adsorption phenomena all over the catalyst surface, resulting in the high anodic current density value at around 2.0 V. In the voltammograms, peak b_1 is ascribed for the oxygen production, and a_2 is considered as hydrogen production peak.

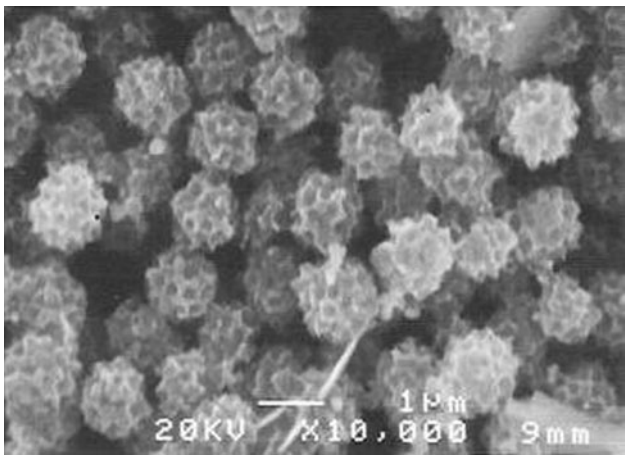

Fig. 4 SEM image of 25 wt% Ni/TiO_2 hollow spheres calcined at 400 °C temperature

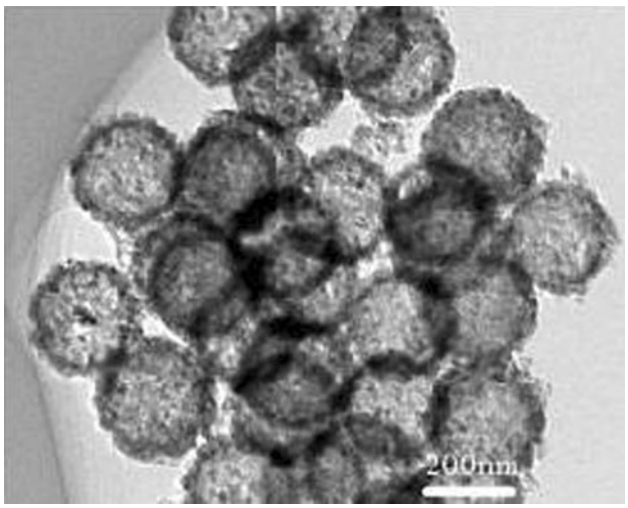

Fig. 5 TEM images of 25 wt% Ni/TiO_2 hollow spheres calcined at 400 °C temperature

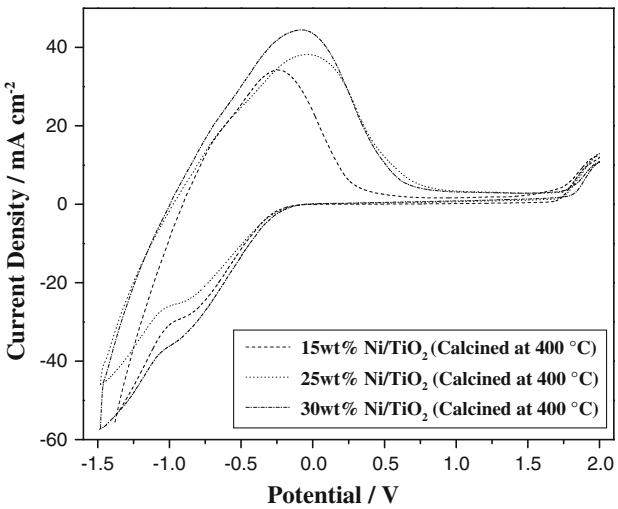

Fig. 6 Cyclic voltammetric results of 15, 25, and 30 wt% Ni/TiO_2 hollow sphere electrocatalysts calcined at 400 °C

It is reported earlier in the literature that, a_1 and a_2 peaks are formed due to the weakly and strongly bonded hydrogen adatoms on the catalyst surface [28, 29]. In the anodic region, peak a_1 is situated almost at the same position ($a_1 \sim -0.085$ V) for 25 and 30 wt% Ni/TiO_2 hollow spheres, whereas for 15 wt% Ni-loaded sample it is formed at the potential of −0.25 V. Actually, this peak is formed due to the hydrogen desorption phenomena at the bulk and surface of the material, which were adsorbed previously. The hydrogen desorption peak is most intense for 30 wt% Ni/TiO_2 catalyst with peak current density of 44.4 mA cm^{-2}, which was in declining order with decrease in the nickel loading, with 38.1 and 34.1 mA cm^{-2} of peak current density value for 25 and 15 wt% Ni-loaded catalysts, respectively. On the other hand, cathodic peak a_2 is assigned for molecular hydrogen production. The cathodic peak current density value is largest for 30 wt% Ni/TiO_2 hollow sphere with 32 mA cm^{-2} value, and further declined for other hollow sphere samples; although the peak position is almost same ($a_2 \sim -0.85$ V) for all the catalysts. It can be concluded from the voltammograms that the electrochemical activity regarding hydrogen desorption and evolution has clearly been increased with inclination of nickel loading over hollow sphere structure. At the same time, oxygen evolution reaction has also been induced by the nickel-doped hollow sphere material, as they have produced approximately 12–13 mA cm^{-2} anodic peak current density. In our previous work, we have seen that titania hollow sphere with 0 % metal loading has produced quite lesser intense cathodic and anodic peak during cyclic voltammetry [20]. Thus, it can be concluded that nickel loading has enhanced the electrocatalytic activity in considerable amount for hydrogen and oxygen evolution during water electrolysis. Among all the nickel-doped electrocatalysts, 30 wt% Ni/TiO_2 hollow sphere sample with calcination of 400 °C has shown the best activity in hydrogen and oxygen evolution reaction. The surface area value with void space created inside the sphere resulted in the high electrocatalytic activity in water electrolysis process.

The cyclic voltammograms of 25 wt% Ni-doped titania hollow sphere were also recorded with various sweep rate (40, 80 and 100 mV s^{-1}), which was represented in Fig. 7. The typical voltammograms are showing the peak current density in increasing order with rise in the sweep rate, although the anodic and cathodic peak positions were almost symmetrical. Figure 8a, b are representing the graph showing the relationship between anodic and cathodic peak currents (i_p) and the square root of the scan rate ($v^{0.5}$) at low and high potential region. Both the figures

are showing linear relationship between i_p and $v^{0.5}$, which concludes the cathodic and anodic peak current is proportional to the square root value of potential scan rate.

The physical and electrochemical characterization results have revealed that the catalysts with more intense NiO phase and less intense rutile TiO_2 phase have worked in hydrogen desorption reaction present in anodic sweep; whereas oxygen evolution peaks are more intense with samples with more intense rutile TiO_2 phase. Thus, it can conclude that the presence of both NiO and TiO_2 phases has contributed in the electrocatalytic activity of hollow sphere samples. It is known from the literature that TiO_2 is oxygen deficient in nature, thus, it could create oxygen vacancies on the catalyst surface, especially on the (110) phase of TiO_2 [30]. On the other hand, nickel monoxide, NiO, exhibits a cubic NaCl structure with a lattice parameter of 0.4173 nm [31, 32]. The NiO always exhibit an excess of oxygen, although the extra oxygen cannot be placed inside the NaCl structure; instead vacancies related to Ni^{2+} are created, thus giving a p-type conduction character [33]. It is known that excess oxygen in NiO produces a Ni^{2+} vacancy, which leads to the creation of a hole on two adjacent Ni^{2+} ions, resulting in the yield of Ni^{3+} ions. Similarly, both the oxides exhibit strong hydrogen adsorption property. Therefore, both oxygen and hydrogen were adsorbed on the hollow sphere surface and also into the void sphere of the samples. From the SEM and TEM images, it is clear that both the gases could enter into the sphere through the pores present all over the sphere. The oxygen adsorption phenomenon at vacancies is resulted in the charge shifting and alteration of the local electronic structure on the semiconductor surface. In the cathodic sweep, oxygen is partially reduced through the interaction of oxygen molecule with Ti^{3+} and Ni^{+} ions,

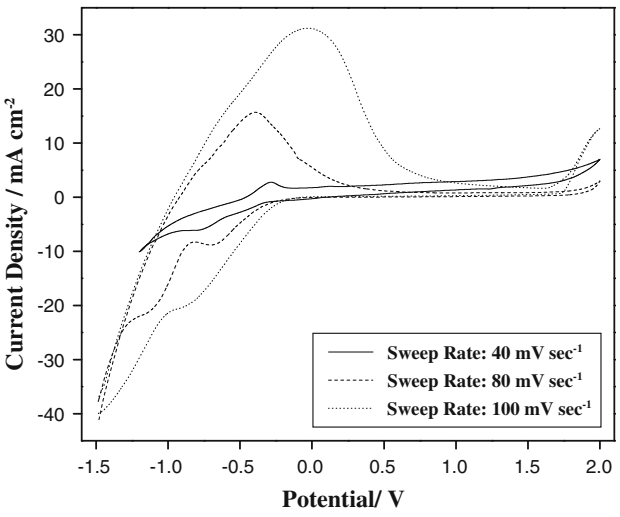

Fig. 7 Cyclic voltammograms of 25 wt% Ni/TiO_2 hollow sphere electrocatalysts at 40, 80, and 100 mV s^{-1} sweep rate

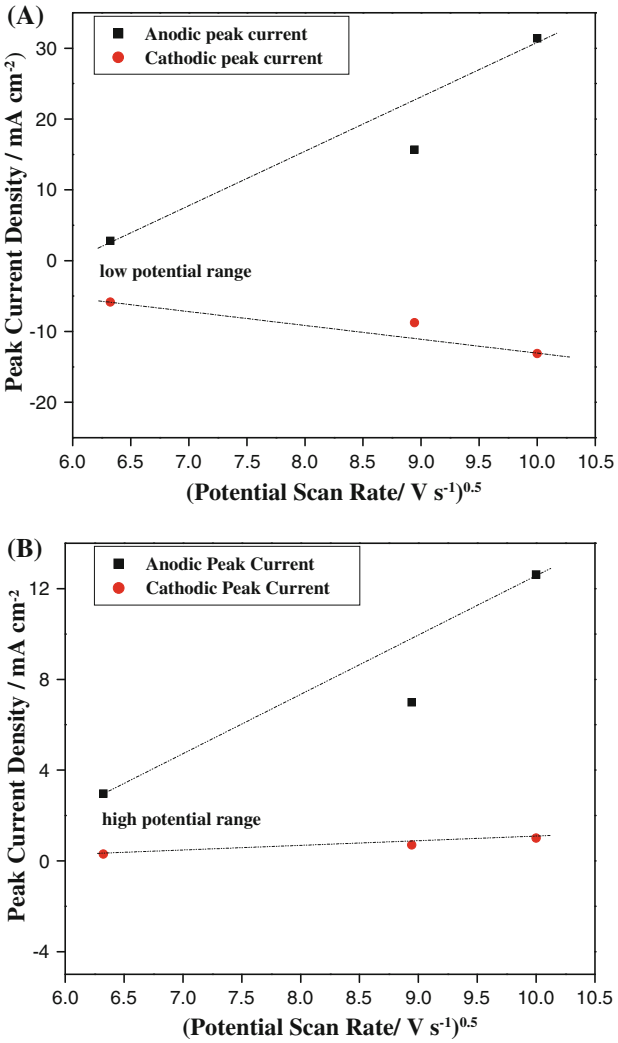

Fig. 8 Relationship between the peak currents and scan rate, $v^{0.5}$ at **a** low potential region, **b** high potential region, for 25 wt% Ni-doped titania hollow sphere calcined at 400 °C

which usually generate at large cathodic potential range. On the catalyst surface, Ti^{4+} and Ni^{2+} matrix are acting as electron excess sites. Thus, oxygen molecules always try to compete for more reduced metal ions, resulting in the unsymmetrical reduction process, with only one oxygen atom bonded to the surface. This oxygen reduction process therefore was resulted in the hydrogen evolution during the electrolysis process.

3.2.2 *Anodic polarization*

The electrocatalytic performance of 15, 25, and 30 wt% Ni-doped titania hollow sphere materials were examined using anodic polarization method by stepping up the potential with potential scan rate of 0.5 mV s^{-1}. The polarization curves presented in the Fig. 9 are showing the anodic current density up to 53 mA cm^{-2} for all the

hollow sphere electrocatalysts. It is evident from the results that the low current cell voltage is almost same for all the electrocatalysts; but at the higher current density range 30 wt% Ni-doped titania hollow sphere sample has shown comparatively lower over potential value. The over potential value was in increasing order with decrease in the nickel loading. Actually, at the lower current density, the performance of the electrocatalysts are not influenced by the ohmic resistivity and high bubble formation. At this range, the over potential value only exhibits due to the anodic reaction performed at the cell. But, at the higher current density range, the over potential value is highly influenced by the ohmic resistivity and bubble formation; thus, it always exhibits in the real operating conditions. Therefore, it is evident from the anodic polarization curves that the electrocatalytic performance was enhanced in the hollow sphere samples with greater loading of nickel.

3.2.3 Tafel plots

Figures 10 and 11 are representing the Tafel plots for hydrogen and oxygen evolution reaction (HER and OER), respectively. Tafel slope can be calculated objectively from the Tafel equation which includes uncompensated ohmic drops:

$$E = a + b\ln I + IR \tag{1}$$

After differentiating Eq. (1) with respect to I will produce:

$$\mathrm{d}E/\mathrm{d}I = b/I + R \tag{2}$$

Thus, the plot of $\Delta E/\Delta I$ versus $1/I$ gives the straight line having slope b and intercept of R. Using this equation, the average value of Tafel slope has been revealed as 86 mV.

3.2.4 Reaction order

Figure 12 is showing the typical plot of log I at $E = 1.5$ V versus pH for 15 and 30 wt% Ni-doped TiO_2 hollow sphere electrocatalysts. The slope of the straight lines will present the reaction order of the system with respect to the H^+ concentration. The average value of -1.42 has been revealed as the reaction order of the system irrespective of the nickel loading and heating duration in the synthesis of hollow sphere materials.

It is known from the literature that reacting particles in O_2 evolution from acid solution are water molecules [34, 35]. Thus, the 1st step will be:

$$H_2O \rightarrow OH_{ad} + H^+ + e^- \tag{3}$$

In our case, this cannot be the rate determining step, otherwise, the reaction order would be zero with respect to H^+. If the second electron transfer will happen in the next step, then the Tafel slope value would be 40 mV. Thus, in the present case, a chemical step would follow the reaction (3). In this mechanism, an unstable OH* intermediate would be produced due to the primary discharge, which will immediately be changed to a more stable OH:

$$H_2O \rightarrow OH*_{ad} + H^+ + e^- \tag{4}$$

$$OH_{ad}* \rightarrow OH_{ad} \tag{5}$$

If a process follows this mechanism, then the Tafel slope would be 60 mV with a reaction order of -1 with respect to H^+. In the present case, with the Tafel slope value of 86 mV, the mechanism would be in mixed form, where reaction (4) will be r.d.s. on a fraction of surface and reaction (3) on the rest of the surface. The observed Tafel slope is resulting from a combination of 120 and 60 mV

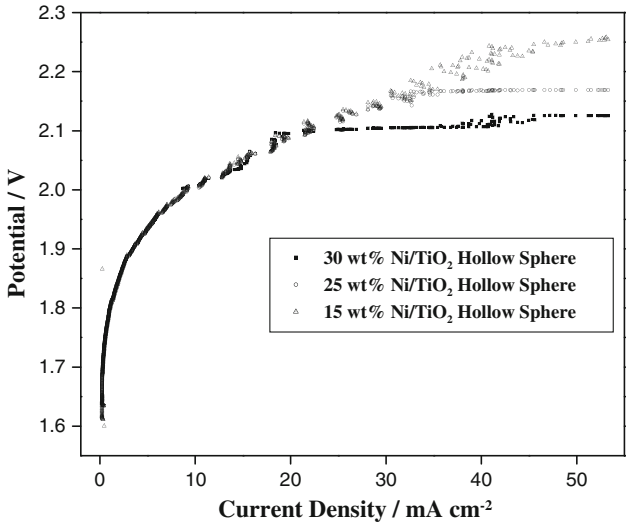

Fig. 9 Anodic polarization curves of 15, 25, and 30 wt% Ni/TiO_2 hollow sphere electrocatalysts calcined at 400 °C temperature

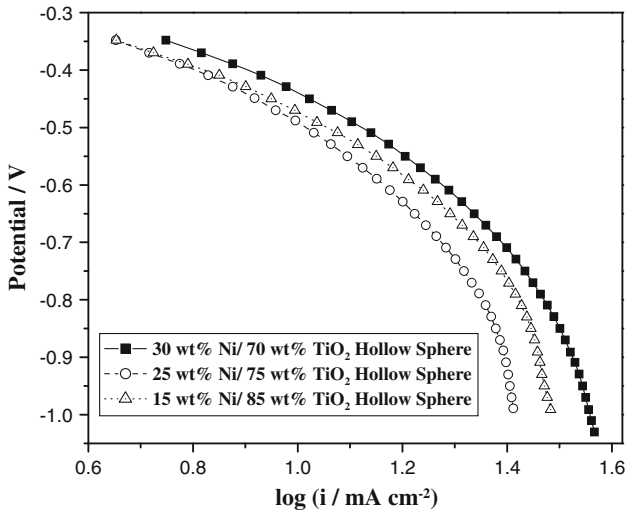

Fig. 10 Tafel plots for H_2 evolution on 15, 25, and 30 wt% Ni-doped titania hollow sphere electrocatalysts

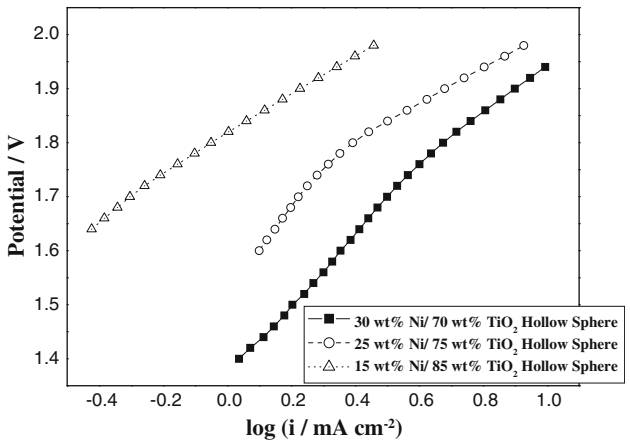

Fig. 11 Tafel plots for O_2 evolution on 15, 25, and 30 wt% Ni-doped titania hollow sphere electrocatalysts

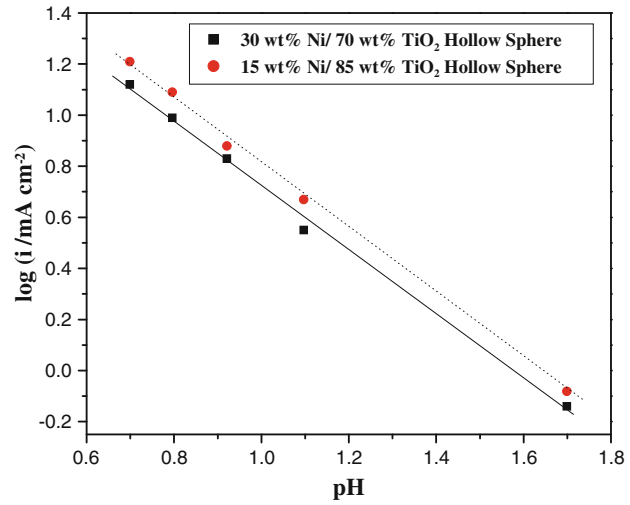

Fig. 12 Determination of reaction order with respect to H^+ for O_2 evolution at $E = 1.5$ V on 15 and 30 wt% Ni/TiO_2 electrocatalysts

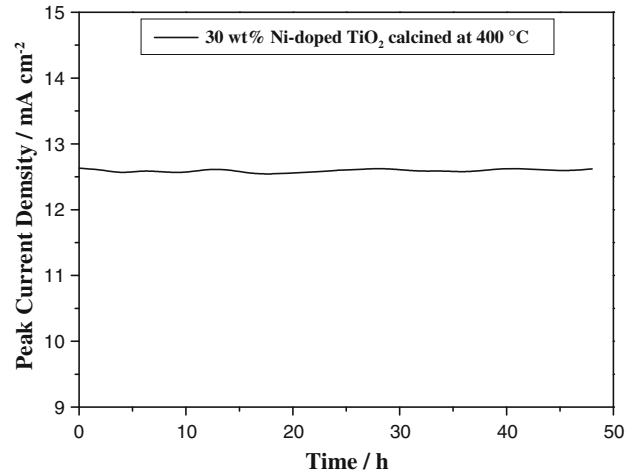

Fig. 13 Stability test—a plot of time versus anodic peak current density for 30 wt% Ni-doped TiO_2 hollow spheres calcined at 300 °C

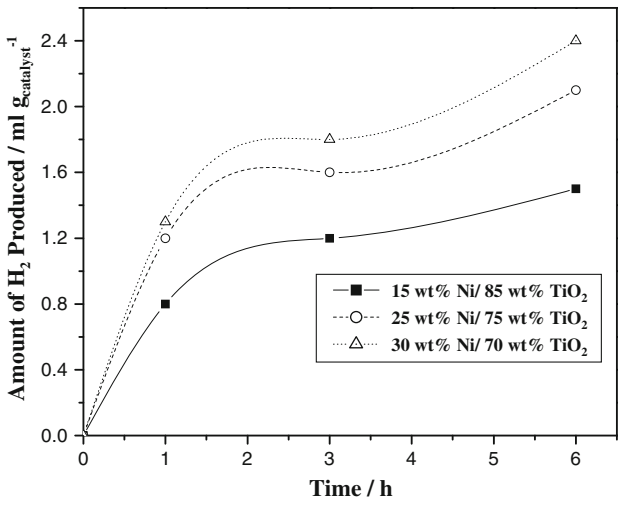

Fig. 14 Photocatalytic hydrogen production using 15, 25, and 30 wt% Ni-doped titania hollow spheres

depending on reaction (4) or (5) being the r.d.s., respectively. The observed Tafel slope of 86 mV supports the above-mentioned mechanism with a reaction order around −1, which also resembles with the actual reaction order value we got experimentally.

3.2.5 Electrocatalyst stability test

The long time electrocatalytic stability test was performed for 30 wt% Ni-doped titania hollow sphere sample at potentiostatic condition, by considering anodic peak current density value from cyclic voltammograms performed every after 2 h for 48 h duration. Figure 13 represents the graph showing anodic peak current density value plotted against time. It is evident from the graph that the Ni/TiO_2 hollow sphere electrocatalysts are stable in electrochemical aspect, as the anodic peak current density value was maintained approximately around 12.5 mA cm^{-2} for all along the experiment duration.

3.3 Photocatalytic hydrogen evolution

Figure 14 represents the photocatalytic hydrogen evolution results with respect to the irradiation time. At all the time intervals, 30 wt% Ni-loaded titania hollow sphere sample has yielded maximum amount of hydrogen during photocatalytic water splitting. The results show that the hollow sphere catalysts with greater nickel loading achieved the greater photocatalytic activity with irradiation for longer duration. The higher activity may be attributed to the combined factors of higher surface area, large pore volume, and void space inside the spheres. Moreover, the results confirmed the strong influence of nickel loading over the hollow spherical structure. The doped metal always plays a pivotal role in charge separation by capturing the electrons.

In the hollow sphere catalysts, Ni^{2+} capture electrons which left freer hole at the inner side of the spheres. Therefore, the holes concentrations increase at the inner side of the spheres, which migrate to the surface layer by withdrawing the electrons from the surface. These phenomena results in the greater photocatalytic activity of the hollow spheres with greater amount of nickel loading.

4 Conclusions

The 15, 25, and 30 wt% Nickel-doped titania hollow spheres were prepared treated with different calcinations temperatures using PSA latex as template material for the hollow spherical structure, and utilized them as electrocatalysts during water electrolysis in acidic media. The hollow spheres were characterized with XRD studies, which revealed the presence of rutile TiO_2 and NiO phases both at the surface and inside the core. The SEM and TEM images have confirmed the hollow spherical structure of the catalysts with average diameter of 0.8–0.9 μm. BET surface area results have shown the highest surface area value of 166.76 $m^2\ g^{-1}$ for 30 wt% Ni/TiO_2 hollow sphere material. Cyclic voltammetric studies have proved the presence of both hydrogen and oxygen evolution peaks for all the hollow sphere samples. The anodic peak current density value, which usually represents the oxygen evolution phenomenon, was revealed as 13 mA cm^{-2} for 25 wt% Ni-loaded sample; whereas the hydrogen evolution peak was most intense for 30 wt% Ni/TiO_2 material with cathodic peak current density of 32 mA cm^{-2}. Similarly, anodic and cathodic peak current density (i_p) has shown linear relationship with the square root of potential scan rate value ($v^{0.5}$) during CV analysis. In anodic polarization curve, the performance of the hollow sphere materials were evaluated up to 53 mA cm^{-2}. Tafel slope value was calculated as 86 mV. The average value of −1.42 has been revealed as the reaction order of the system irrespective of the nickel loading and heating duration in the synthesis of hollow sphere materials. During photocatalytic water splitting, 30 wt% Ni/TiO_2 hollow sphere sample has yielded the highest amount of hydrogen in all irradiation time span.

References

1. Patterson J, Ramsey B, Harrison D. http://dspace.brunel.ac.uk/bitstream
2. Friedland R, Speranza AJ (1999) DOE Hydrogen program review. In: Proceedings of the 1999 U.S., vol 1. National Renewable Energy Laboratory No. NREL/CP-570-26938 Golden, Colorado
3. Peavey M (2003) Fuel from water energy impendence with hydrogen. Merit Products, USA
4. Chandler GK, Genders JD, Pletcher D (1997) Platinum Metals Rev 41:54–63
5. Reinhardt D, Krieck S, Meyer S (2006) Electrochim Acta 52:825–830
6. Bamwenda GR, Ueisigi T, Abe Y, Sayama K, Arakwa H (2001) Appl Catal A 205:117–128
7. Contescu C, Popa VT, Miller JB, Ko EI, Schwarz JA (1996) Chem Eng J Biochem Eng J 64:265–272
8. Odobel F, Blart E, Lagree M, Villieras, Boujtita N, Murr E, Caramori S, Bignozzi CA (2003) J Mater Chem 13:502–510
9. Pessoa CA, Gushikem Y, Nakagaki S (2002) Electroanalysis 14:1072–1076
10. Pessoa CA, Gushikem Y (1999) J Electroanal Chem 477:158–163
11. Yoshihiko K, Yoshikawa H, Agwa K, Murayama M, Mori T, Sunada K, Bandow S, Ijima S (2008) Langmuir 24:547–550
12. An K, Lee N, Park J, Kim CS, Hwang Y, Park JG, Kim JY, Park JH, Han JM, Yu J, Hyeon T (2006) J Am Chem Soc 128:9753–9760
13. Graf C, Dembski S, Hofmann A, Ruhl E (2006) Langmuir 22:5604–5610
14. Zhu YZ, Chen HB, Wang YP, Li ZH, Cao YL, Chi YB (2006) Chem Lett 35:756–757
15. Fujiwara M, Shiokawa K, Hayashi K, Morigaki K, Nakahara Y, Biomed J (2007) Mater Res A 81:103–112
16. Shiho H, Kawahashi N (2000) J Colloid Interface Sci 226:91–97
17. Kawahashi N, Shiho H (2000) J Mater Chem 10:2294–2297
18. Yoon SB, Kim JY, Kim JH, Park SG, Kim JY, Lee CW, Yu JS (2000) Curr Appl Phys 6:1059–1063
19. Wang C, Ao Y, Wang P, Hou J, Qian J, Zhang S (2010) J Hazard Mater 178:517–521
20. Chattopadhyay J, Kim HR, Moon SB, Pak D (2008) Int J Hydrogen Energy 33:3270–3280
21. Son JE, Chattopadhyay J, Pak D (2010) Int J Hydrogen Energy 35:420–427
22. Tucker SH (1950) J Chem Ed 27:489
23. Changwei X, Yonghong H, Rong J, Jiang SP, Yingliang L (2007) Electrochem Commun 9:2009–2012
24. Nishida R, Kakinuma K, Nishino H, Kamino T, Yamashita H, Watanabe M, Uchida H (2009) Solid State Ionics 180:968–972
25. Mahesh RA, Jayaganthan R, Prakash S, Chawla V, Chandra R (2009) Mater Chem Phys 114:629–635
26. Kim H, Eom Y, Lee T, Shul Y (2008) Mater Chem Phys 108:154–159
27. Gregg SJ, Sing KSW (1982) Adsorption, surface area and porosity, 2nd edn. Academic Press, New York
28. Woods R (1976) In: Bard A (ed) Chemisorption at electrodes in electroanalytical chemistry, vol 9. Marcel Dekker, New York
29. Czerwinski A (1994) J Electroanal Chem 379:487–493
30. Diebold U (2003) Surf Sci Rep 48:53–229
31. Niklasson GA, Granqvist CG (2007) J Mater Sci 17:127–156
32. Lide DR (2000) CRC handbook of chemistry and physics, 73rd edn. CRC Press, Boca Raton
33. Lunkenheimer P, Loidl A, Ottermann CR, Bange K (1991) Phys Rev B 44:5927–5930
34. Trasatti S (1990). In: Wendt H (ed) Electrochemical hydrogen technologies Elsevier, Amsterdam, p 104
35. Hrussanova A, Guerrini E, Trasatti S (2004) J Electroanal Chem 564:151–157